energies

MDPI

Article

Phenyl Vinylsulfonate, a Novel Electrolyte Additive to Improve Electrochemical Performance of Lithium-Ion Batteries

Behrooz Mosallanejad [1], Mehran Javanbakht [1,2,*], Zahra Shariatinia [1] and Mohammad Akrami [3,*]

[1] Department of Chemistry, Amirkabir University of Technology (Tehran Polytechnic), Tehran 159163-4311, Iran
[2] Renewable Energy Research Center, Amirkabir University of Technology, Tehran 15916-34311, Iran
[3] Department of Engineering, University of Exeter, Exeter EX4 4QF, UK
* Correspondence: mehranjavanbakht@gmail.com (M.J.); m.akrami@exeter.ac.uk (M.A.)

Abstract: Irreversible capacity fading, originating from the formation of the solid electrolyte interphase (SEI), is a common challenge encountered in lithium-ion batteries (LIBs) containing an electrolyte based on ethylene carbonate (EC). In this research, phenyl vinyl sulfonate (PVS) is examined as a novel electrolyte additive to mitigate this issue and subsequently enhance the cyclic stability of LIBs. As evidenced by density functional theory (DFT) calculations, PVS has a higher reduction potential than that of EC, which is in accordance with the cyclic voltammetry (CV) measurements. Accordingly, the PVS-containing electrolyte demonstrated a reduction peak at ~1.9 V, which was higher than that of the electrolyte without an additive (at ~1.7 V). In contrast to the SEI derived from the reference electrolyte, the one built-in PVS-containing electrolyte was capable of completely inhibiting the electrolyte reduction. In terms of the Raman spectroscopy and electrochemical impedance spectroscopy (EIS) analysis, SEI formation as the result of PVS reduction can lead to less structural disorder in the graphite electrode; the battery with the additive showed less interfacial and charge transfer resistance. The Li/graphite cell with 1 wt % of PVS delivered capacity retention much higher than that of its counterpart without the additive after 35 cycles at 1 C.

Keywords: lithium-ion battery; graphite anode; electrolyte additive; solid electrolyte interphase; phenyl vinyl sulfonate

Citation: Mosallanejad, B.; Javanbakht, M.; Shariatinia, Z.; Akrami, M. Phenyl Vinylsulfonate, a Novel Electrolyte Additive to Improve Electrochemical Performance of Lithium-Ion Batteries. *Energies* **2022**, *15*, 6205. https://doi.org/10.3390/en15176205

Academic Editor: Wan Jefrey Basirun

Received: 1 August 2022
Accepted: 23 August 2022
Published: 26 August 2022

1. Introduction

In the last few decades, concerns about the rise in the production of greenhouse gases caused by the burning of fossil fuels have driven scientists to explore clean and durable energy resources [1–6]. The necessity of such a crucial exploration is to employ energy storage devices, one of which is the lithium-ion battery (LIB) [7]. LIBs are broadly employed as power sources in portable devices, such as laptop computers, and are also found in electric vehicles [8,9]. Conventional LIBs are made up of a graphite anode along with a transition metal oxide cathode, immersed in an organic electrolyte and separated by a separator [10].

From the beginnings of battery development until the present, anode materials have been one of the most controversial topics in the field of batteries [11]. Prior to the advent of up-to-date LIBs, lithium (Li) has been used as an anode. Because of safety issues ensuing from dendrite formation in lithium metal batteries, this anodic material was later replaced with carbon-intercalation materials [12–14]. Because of its merits, including high stability and theoretical specific capacity, accompanied by low electrode potential, graphite is commonly used as an anodic material in LIBs [15]. One of the main challenges encountered with a graphite electrode is its low compatibility with a non-aqueous electrolyte, which arises from its operating potential window [16]. In propylene carbonate (PC)-based electrolytes, the exfoliation of graphite takes place owing to the generation of propylene gas [17,18]. In contrast, in ethylene carbonate (EC)-based electrolytes, the formation of a passivation layer, called solid electrolyte interphase (SEI), occurs between the graphite anode and the

electrolyte, which enables the battery to charge and discharge consecutively [16,18]. The formation of the SEI layer occurs during the initial charging of the LIB, through the decomposition of the electrolyte [16]. According to Figure S1 in the Supplementary Materials, the non-aqueous electrolyte is not thermodynamically stable on the surface of the graphite electrode; therefore, SEI formation happens as the result of the electrolyte decomposition in the potential ranging from 0.6 to 1.3 V vs. Li^+/Li. In EC-based electrolytes, an irreversible loss of capacity is observed, which stems from the consumption of Li^+ ions in the SEI formation process [16].

One of the most cost-effective and advantageous avenues explored to promote the compatibility of graphite electrodes with PC-based electrolytes, as well as in EC-based electrolytes, is the usage of electrolyte functional additives or SEI additives. In PC-based electrolytes, the usage of SEI additives is indispensable for better cell performance because the SEI layer that arises from the additive will not only rescue the graphite anode from exfoliation but can also enable the LIB to charge and discharge in subsequent cycles. In EC-based electrolytes, the role of SEI additives is different; they improve the cell's performance by modifying the nature of the SEI layer [19–21].

SEI additives have lower reduction potentials in comparison with the electrolyte solvents, which enables them to reduce prior to the decomposition of the electrolyte solvents and to generate a robust and uniform SEI layer on the graphite electrode's surface (see Figure S1 in the Supplementary Materials) [22]. One of the main types of electrolyte functional additives is the reduction-type additives. The most important characteristic of this type of additive is that they offer one or more double or triple bonds to supply a site suitable for polymerization in the reductive reaction. Electrochemically induced polymerization is involved in the mechanism of SEI formation in these additives (see Figure S2 in the Supplementary Materials) [20,21].

Among the reduction-type additives, vinylene carbonate (VC) is the most well-known and commonly used additive in LIBs [21]. Allyl ethyl carbonate (AEC) is another reduction-type additive that was adopted to inhibit the exfoliation of the graphitic anode, due to its higher reduction potential with respect to the PC, as well as its ability to build a stable SEI layer. The cell with 2 wt % of AEC demonstrated a reversible capacity of 320 mAh g^{-1} after 10 cycles [23]. In an earlier study, Wagner et al. [24] investigated the effect of methyl vinyl sulfone (MVS) and ethyl vinyl sulfone (EVS) additives on the electrochemical performance of LIB. They realized that the MVS and EVS additives offer the lowest unoccupied molecular orbital (LUMO) energy levels compared to PC, which allows them to undergo reduction before the PC decomposition process and to suppress the exfoliation of the graphite anode through the formation of a stable SEI layer [24]. In addition to the role of these additives to prevent the exfoliation of graphitic anodes in PC-based electrolytes, they can also be employed for EC-based electrolytes in order to improve the cyclability of LIBs. As reported in the study by Komaba et al. [25], the formation of a poly(2-vinyl pyridine) film via the electrochemical reductive polymerization of a 2-vinyl pyridine (VP) additive on a graphite electrode can hamper the electro-reduction of the manganese ions (Mn^{2+}) on the electrode's surface, which may result in an improvement of the electrochemical performance of the graphite/$LiMn_2O_4$ full-cell [25].

For the first time, in this study, we introduce phenyl vinyl sulfonate (PVS) as a novel electrolyte additive for LIBs that is functionalized with the sulfonate (-OSO_2-) and vinyl (C=C) chemical groups. Density functional theory (DFT) calculations demonstrate that PVS possesses a higher reduction potential (RP) than that of the EC solvent; thus, we believe that this compound can reduce before the decomposition of EC, which subsequently modifies the surface of the graphite electrode and affects the LIB's performance. Varied surface characterization tests, along with electrochemical measurements, are conducted to examine the morphology and chemistry of the PVS-driven SEI layer and its impact on the electrochemical performance of Li/graphite cells.

2. Materials and Methods

2.1. Theoretical Calculations

The DFT calculations of the redox potentials of EC and PVS molecules, as illustrated in Figure 1, were performed using the program package, Gaussian 09 [26]. All the calculations were performed by means of the B3PW91 functional and 6-311G (d,p) basis set. The procedure used for the calculation of oxidation potential (OP) and the reduction potential (RP) of the molecules were thoroughly discussed in our previous work [27].

2.2. Electrolyte Preparation

EC (Merck, for synthesis), dimethyl carbonate (DMC) (Merck, for synthesis), lithium hexafluorophosphate salt ($LiPF_6$) (Sigma-Aldrich, battery grade), and PVS (Sigma-Aldrich, 95%) as the case-study additive were used as received. First, 1 M $LiPF_6$, dissolved in EC:DMC (1:1, v/v), was used as the "reference" electrolyte. To desiccate the moisture present in the solvents, 4 Å molecular sieves were dehumidified at 350 °C for 17 h. Then, the solvents were stored over arid molecular sieves under high-purity argon in a glove box for several days. The water amount of the prepared electrolytes was determined by Karl Fischer titration (Mettler Toledo DL31), which was <10 ppm.

2.3. Electrode Preparation and Cell Assembling

The commercial graphite electrodes used in this work were composed of graphite powder (93 wt %, as the active material), styrene-butadiene rubber (SBR) (4.6 wt %, as the binder), carboxymethyl cellulose (CMC) (1.4 wt %, as the binder), and Super P (SP) (1 wt %, as the conductive additive), with copper (Cu) foil as the current collector. The graphite electrode, a micro-pore polypropylene membrane (Celgard 2400) acting as the separator, and Li foil, acting as the counter electrode, were assembled into coin cells in a glove box filled with argon (Ar) gas.

2.4. Electrochemical Measurements

The charge-discharge experiments were conducted by employing a battery tester (Kimiastat-5V/10 mA, Kimia Pardaz Rayane, Iran). In order to investigate the cathodic stability of the case-study electrolytes, cyclic voltammetry (CV) measurements were executed at a scan rate of 0.1 mV s^{-1} from 0.001 to 3 V (vs. Li^+/Li). Moreover, the anodic behavior of electrolytes was examined by means of a linear sweep voltammetry (LSV) test at a scan rate of 0.1 mV from 3 to 6 V vs. Li^+/Li, using a three-electrode cell consisting of a Pt electrode as the working electrode and Li foils as the counter and reference electrodes. In electrochemical impedance spectroscopy (EIS) analysis, a 10 mV excitation potential and a frequency varying from 100 kHz to 0.1 Hz were applied. All the CV, LSV, and EIS measurements were carried out with a Galvano-stat/Potentio-stat Autolab (PGSTAT 302N) at room temperature.

2.5. Surface Analyses of the Electrode

The formation process of an SEI film on a graphite electrode's surface was achieved using five charge-discharge cycles at a low C-rate (0.1 C) from 0.001 to 3 V (vs. Li^+/Li). After formation, the coin cells were dismantled in a glove box filled with Ar gas, then the graphite electrodes were rinsed with DMC solvent, followed by vacuum drying for several hours before analysis. The morphology and chemical composition investigation of the graphite anode surface were performed using field-emission scanning electron microscopy (FE-SEM) (Tescan Mira 3-LMU, 15 kV) and an energy-dispersive spectrometer (EDS) mounted on FE-SEM, respectively. To characterize the organic functional groups available on the graphite electrode's surface, a Bruker Alpha Fourier-transform infrared (FT-IR) spectrometer was hired. Raman spectra of the graphite electrodes were obtained through a Takram Raman microscope, using a 532 nm Nd:YAG laser. To carry out the UV-visible spectroscopy, after washing and drying, the arid electrodes were soaked in

a specified amount of methanol for four days. The UV-visible absorption spectra were recorded in ambient air using a Perkin Elmer Lambda 45 spectrometer.

3. Results and Discussion

3.1. DFT Calculations

The RP and OP of the EC and PVS molecules are shown in Figure 1. An SEI-forming additive should have a higher RP than that of an electrolyte solvent, meaning that the additive is capable of reducing prior to the reduction of solvent and to forming an SEI layer on the electrode [10,27]. Accordingly, the PVS molecule has a higher RP than that of the EC, implying that this molecule is expected to reduce before the EC and to act as an SEI additive. Moreover, this molecule has a lower OP compared to the EC solvent, which shows its lower anodic stability than that of EC [10,27].

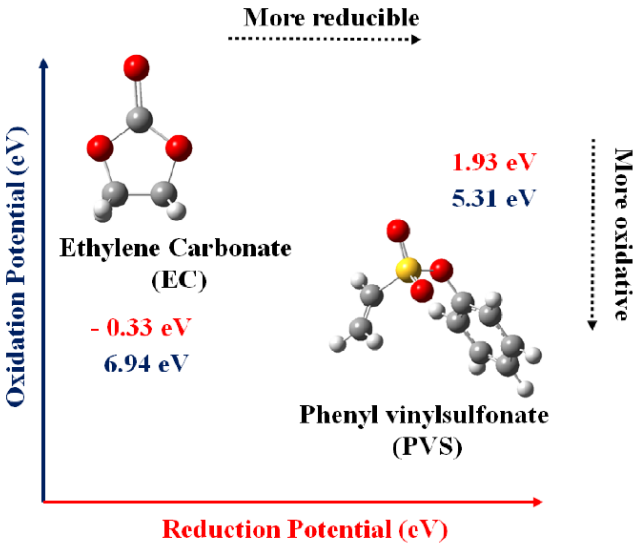

Figure 1. The oxidation and reduction potentials of EC and PVS.

3.2. Electrochemical Study

3.2.1. Charge-Discharge Test

In order to optimize the PVS content in the reference electrolyte, the effect of various doses of additive on the electrochemical performance of LIB was examined, as shown in Figure S3 in the Supplementary Materials. In addition, the charge and discharge capacities, as well as the Coulombic efficiency (CE) of these samples, are listed in Table 1. The long voltage plateau, varying from 0.2 to 0.01 V, in the discharge curve is related to the lithium intercalation process [28]. The CE of the LIB with the reference electrolyte is 69.3%, while the inclusion of 1% wt PVS into the reference electrolyte increased the CE of the LIB to 80.9%. Interestingly, by increasing the additive amount, a decrease in CE was observed, corresponding to the generation of a thicker SEI layer on the surface of the graphite electrode and, subsequently, higher interfacial resistance [28,29]. Consequently, 1 wt % of PVS was chosen as the optimal amount of additive in the reference electrolyte.

Figure 2 illustrates the capacity retention of Li/graphite cells containing the reference electrolyte and 1 wt % of PVS electrolyte, after 35 cycles at 1 C from 0.001 to 3 V at room temperature. The capacity retention of the reference cell decreased to only 50.4% of retention in comparison with its initial discharge capacity, whereas the cell with 1 wt % of PVS delivered superior cycle stability, accompanied by an excellent cycling performance. The good electrochemical performance of the cell with 1% wt of PVS testifies to the important role of the additive in building a stable SEI layer that can hinder the continuous consumption of Li^+ ions arising from the formation of an imperfect SEI layer by the reference electrolyte.

Table 1. The charge capacity, discharge capacity, and CE of the Li/graphite half-cells containing various doses of PVS.

Samples	Discharge Capacity (mAh g^{-1})	Charge Capacity (mAh g^{-1})	Coulombic Efficiency (%)
no additive	481.4	333.6	69.3
1% PVS	328.4	256.9	80.9
2% PVS	278.1	196.4	70.6
3% PVS	287.2	153.1	53.3
4% PVS	147.7	50.3	34.1
5% PVS	76.9	22.4	29.2

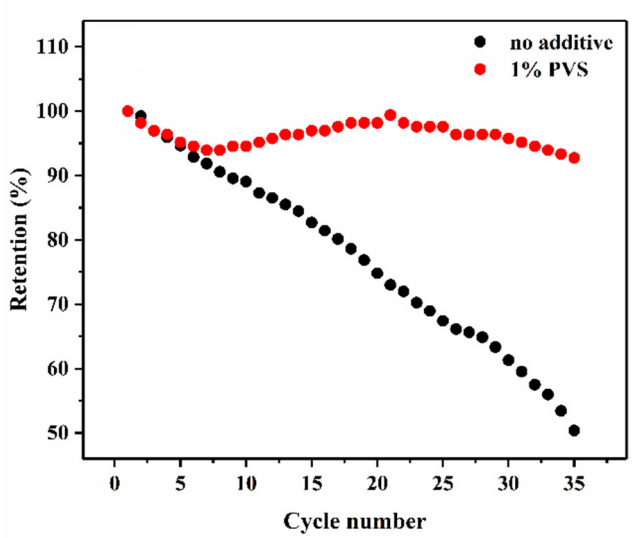

Figure 2. The capacity retention of the Li/graphite half-cells without and with the PVS additive after 35 cycles at the C-rate of 1 C and in the voltage range of 0.001–3 V.

3.2.2. CV Measurements

The CV curves of Li/graphite cells containing the reference and 1 wt % of PVS electrolyte during the first and second cycles are shown in Figure 3a,b. A reduction peak appears in the first cathodic potential sweep of the reference electrolyte at ~1.7 V, which is associated with the reduction of the electrolyte and the formation of an SEI layer (Figure 3a). The point here is that the reduction peak at ~1.7 V appears again, implying that the SEI derived from the reference electrolyte could not completely suppress the further reduction of electrolyte in the subsequent cycle. As can be seen in Figure 3b, by adding 1 wt % of PVS into the reference electrolyte, its cathodic behavior was changed. In the first cathodic potential sweep of 1 wt % of the PVS electrolyte, a reduction peak was observed at ~1.9 V, arising from a reduction in the PVS additive, a peak that is higher than that of the reference electrolyte. Interestingly, the reduction peak related to the reference electrolyte at ~1.7 V was not observed in the first and second cycles, which highlights the role of the PVS-derived SEI layer in completely suppressing the electrolyte reduction and subsequent capacity loss. The cathodic peak below 0.25 V is associated with the intercalation of Li^+ ions into the graphite [30]. Comparing the lithiation/de-lithiation peaks of Li^+ ions in the CV curves of the electrolytes highlights the finding that their intensities in the 1% PVS electrolyte are higher than those in the reference electrolyte, showing that the addition of PVS reduced the polarization in LIB [28].

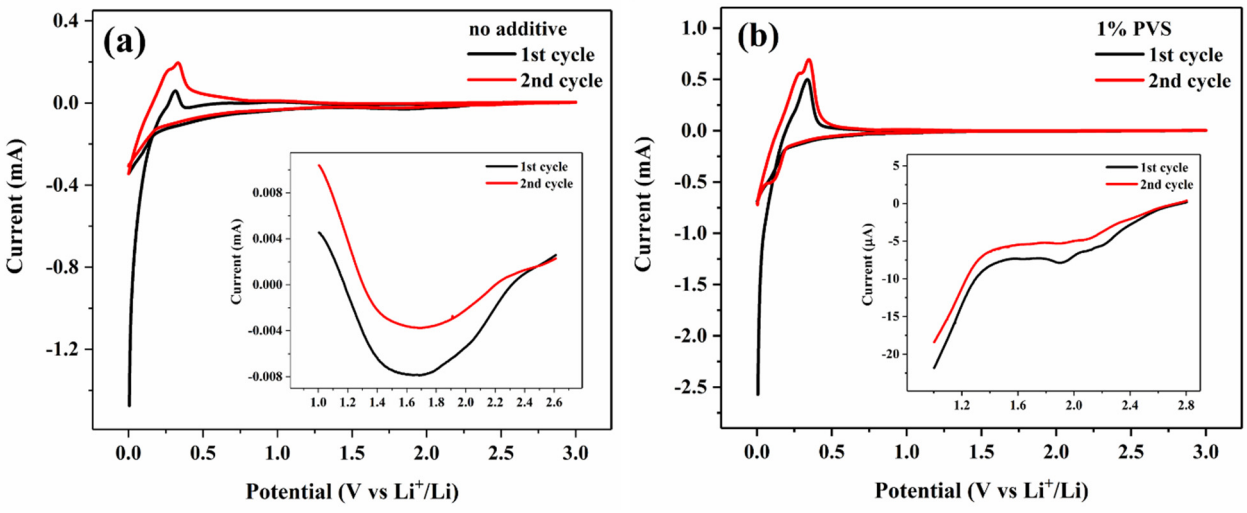

Figure 3. The CV curves of the Li/graphite half-cells in the (**a**) electrolyte without additive and (**b**) electrolyte containing 1 wt % of PVS.

3.2.3. LSV Measurements

Figure 4 depicts the LSV curves of the electrolyte samples without and with the additive. While the electrolyte without the additive is stable up to ~5 V, the other electrolyte shows an increased oxidation current at ~4.3 V. Therefore, the PVS additive shows less anodic stability compared to EC, which is consistent with the DFT calculations.

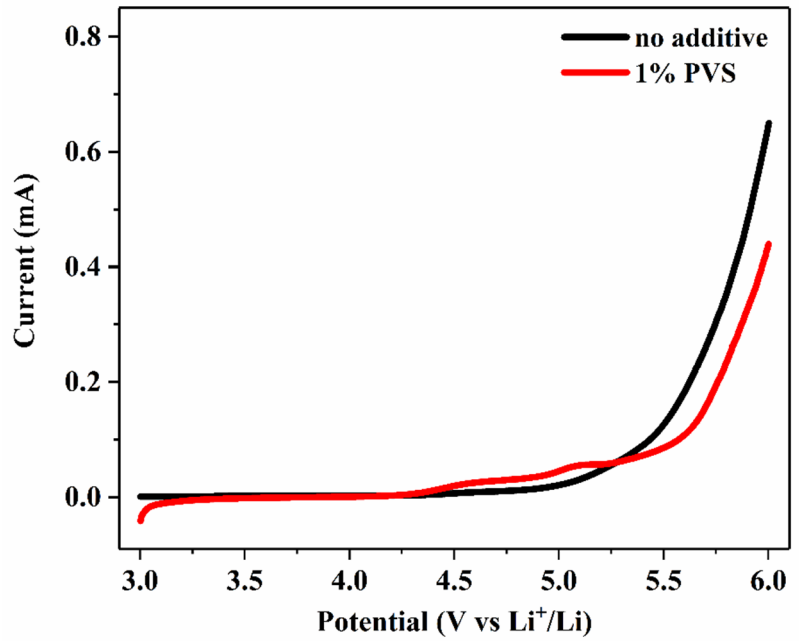

Figure 4. The LSV curves of the electrolytes without and with 1 wt % of the PVS.

3.2.4. EIS Analysis

Figure 5a,b illustrates the EIS curves of Li/graphite cells after 5 cycles at 0.5 C and 50 cycles at 1 C, containing electrolytes without and with the PVS additive. A typical Nyquist plot of LIBs is composed of a semicircle at a high frequency that can be ascribed to the interfacial layer resistance (R_f), a semicircle located at a medium frequency that is relevant to the charge transfer resistance (R_{ct}) and the Warburg impedance (W_0), which can be imputed to the solid phase diffusion of Li^+ ions in the bulk of the intercalation compound [31,32].

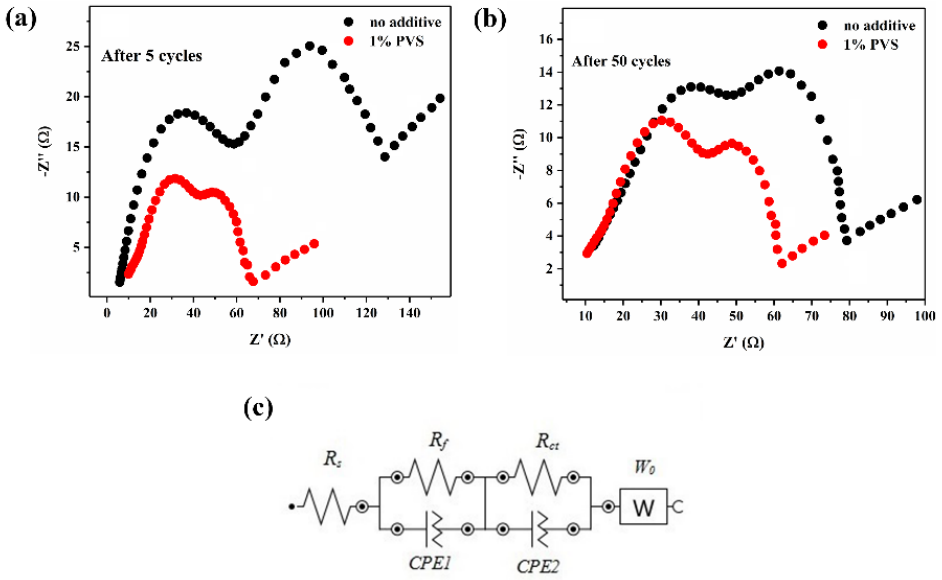

Figure 5. The Nyquist curves of Li/graphite half-cells without and with 1% PVS after (**a**) 5 cycles of 0.5 C as the formation, and (**b**) after 50 cycles of 1 C. (**c**) The equivalent circuit adopted for simulating the experimental results.

The data obtained from the fitting of the EIS curves of the reference and 1% PVS electrolytes by means of the equivalent circuit shown in Figure 5c are reported in Table 2. Accordingly, the electrolyte containing 1 wt % of PVS shows lower interfacial and charge transfer resistance compared to the one without an additive after 5 and 50 cycles, implying that the addition of PVS into the electrolyte resulted in the formation of a favorable SEI film. The lowered interfacial and charge transfer resistance could decrease the ohmic and activation polarization occurring during the insertion/de-insertion of Li^+ ions into the electrode, giving rise to the superior cyclic stability of the electrode [31,33].

Table 2. Data obtained from the fitting EIS diagrams of the electrodes cycled in the electrolytes without and with 1 wt % of PVS after 5 cycles at 0.5 C and 50 cycles at 1 C.

Sample	*After 5 Cycles*			*After 50 Cycles*		
	R_s (Ω)	R_f (Ω)	R_{ct} (Ω)	Rs (Ω)	R_f (Ω)	R_{ct} (Ω)
No Additive	5.88	52.87	68.09	12.24	35.15	34.6
1% PVS	9.91	33.29	24.44	10.44	31.99	19.72

3.3. Structural Analyses

3.3.1. SEM and EDX Analyses

The SEM micrographs of the graphite anodes before cycling, assigned as the "fresh electrode" and after the formation process in both electrolytes without and with the additive are shown in Figure 6. The clean and smooth sheets of the graphite anode are clearly visible in Figure 6a. After their formation, a change was observed in the morphology of the graphite anodes; some of the reductive decomposition products of the electrolyte can be observed on the surface of the anodes (Figure 6b–d). Because of the facile reduction of the electrolyte with PVS compared to the reference electrolyte, different morphologies can be observed.

Elemental analysis of the interfacial layer formed on the surface of the graphite anode was performed using EDS; the patterns for both electrolytes are shown in Figure 7. The well-defined sulfur peak at ~2 keV in the electrode with the PVS is related to the sulfurous compounds arising from the decomposition of PVS, whereas this peak is not found for the electrolyte without additive [34], testifying to the role of the additive in building an SEI layer on the surface of the graphite anode.

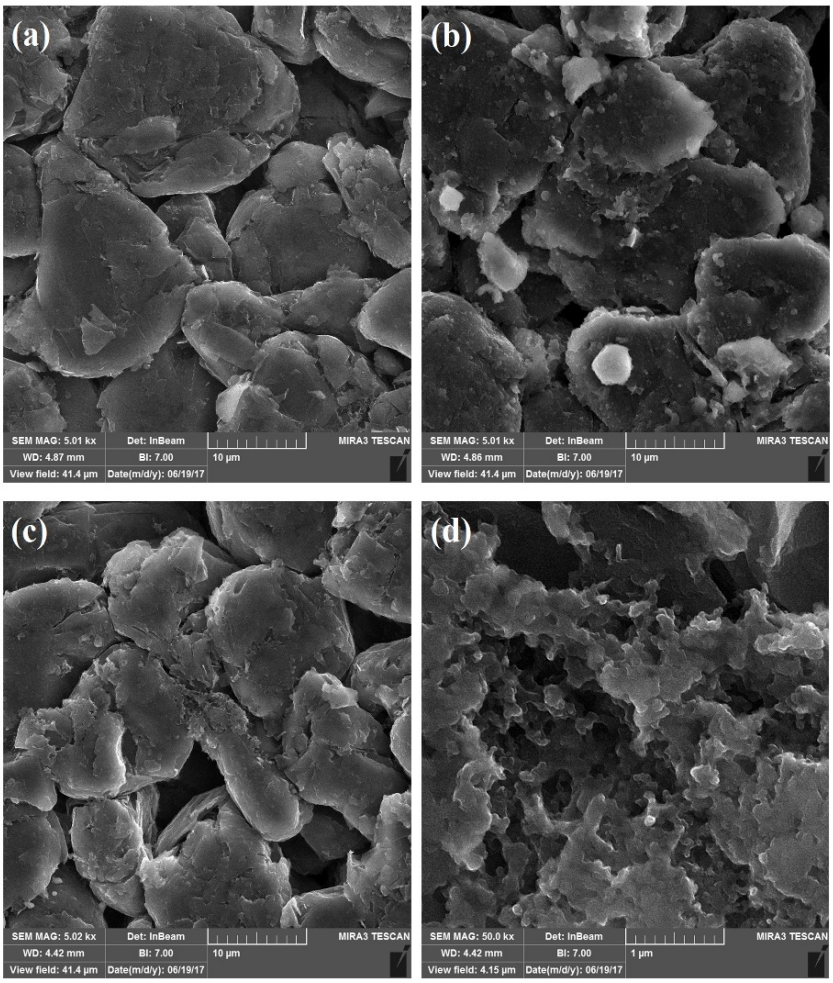

Figure 6. The SEM images that were taken from the graphite electrodes: (**a**) before cycling (fresh electrode), (**b**) after cycling in the electrolyte without the PVS, (**c**,**d**) after cycling in the electrolyte with the PVS at two different magnifications.

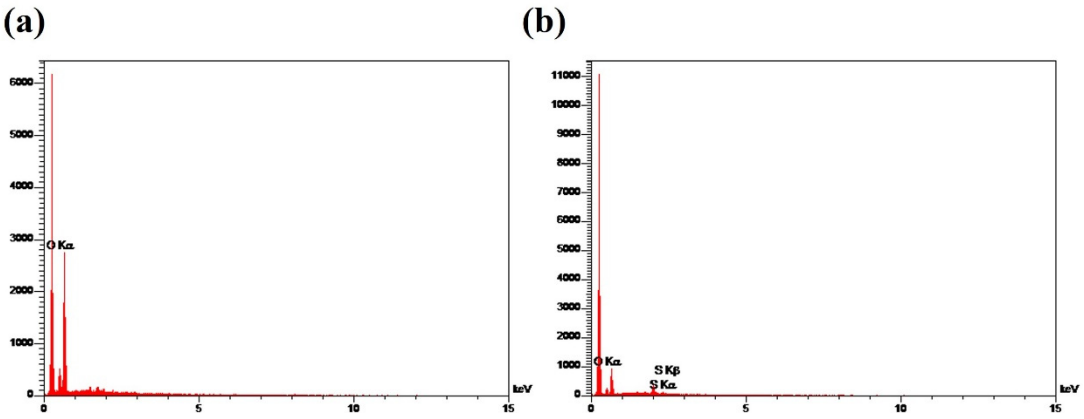

Figure 7. EDS patterns recorded for the graphite electrodes, cycled in (**a**) the electrolyte without the PVS, and (**b**) the electrolyte with 1 wt % of the PVS.

3.3.2. FT-IR Spectroscopy

Figure 8a illustrates the FT-IR spectra of the electrodes cycled in the electrolytes without and with PVS. The peaks found at 1630 cm^{-1} ($\upsilon_{asC=O}$) and 1080 cm^{-1} (υ_{C-O}) can be imputed to the lithium alkyl carbonate species, including lithium ethylene decarbonate (LEDC) and lithium methyl carbonate (LMC). The peaks observed at 1481 cm^{-1} ($\delta_{CH3,CH2}$)

and 841 cm^{-1} ($\delta_{CO3}{}^{2-}$) stem from the presence of Li_2CO_3 [35–37]. As reported in the literature, EC can take part in the generation of an SEI layer through two mechanisms. In the first mechanism, an electrochemically induced reduction of EC occurs, leading to the production of lithium carbonate (Li_2CO_3) along with gaseous products. In the second mechanism, an SEI layer showing more stability is formed, which is mainly made up of LEDC [20,38]. The reduction of DMC as the co-solvent, as used in our study, brings about the production of LMC [39]. In the spectrum of the electrode cycled in the electrolyte with PVS, a pronounced peak is seen at 1312 cm^{-1} that is related to the asymmetric SO_2 stretching, which evidences the presence of the reductive products of the PVS in the SEI layer [40,41].

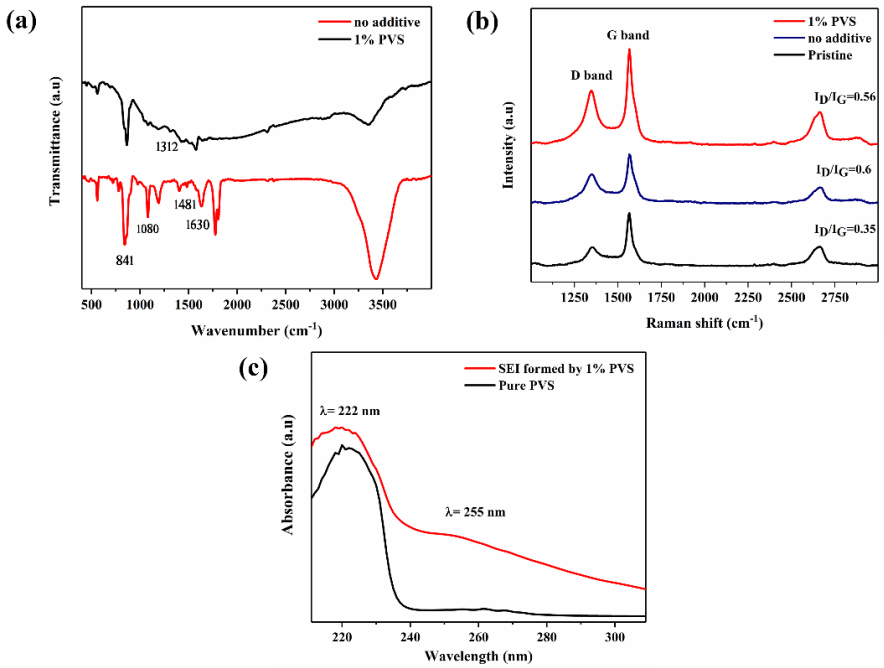

Figure 8. (**a**) The FT-IR spectra of the graphite electrodes after cycling in the electrolyte without and with the additive, (**b**) Raman spectra of the fresh and the cycled graphite electrodes in the electrolytes without and with the PVS, (**c**) UV-visible spectra of the PVS powder (pure PVS) and the SEI formed on the graphite electrode's surface through the reduction of the PVS.

3.3.3. Raman Spectroscopy

Figure 8b shows the Raman spectra of the electrodes before cycling and after cycling in electrolytes without and with PVS. The Raman spectrum of the graphite electrode is commonly composed of two distinct peaks, including the D-band and G-band. The former appears at ~1380 cm^{-1} and is related to the A_{1g} vibrational mode; it can be assigned to the breathing motion of sp^2 hybridized carbon atoms in the rings at the edge planes and to defects in the graphite sheets. The latter peak located at ~1580 cm^{-1} can be imputed to the E_{2g} vibrational mode and corresponds to the relative motion of the sp^2 carbon atoms in the rings and chains. The peak intensity between D-band and G-band (I_D/I_G) has been adopted to determine the degree of structural disorder in the graphite electrode, whereas this ratio is at zero for intact graphite [40,42,43]. The I_D/I_G ratio is 0.35 for a fresh graphite electrode, attesting to the presence of defects and disorders in the graphite structure. The I_D/I_G ratio for the electrode that was cycled in the electrolyte containing the PVS was less than that of its counterpart devoid of the additive, indicating that the SEI film built in the electrolyte with the PVS is more efficient in terms of protecting the surface structure of the graphite electrode [33].

3.3.4. UV-Visible Spectra

Figure 8c shows the UV-visible spectra of the PVS powder and the graphite electrode that was cycled in the electrolyte containing the PVS. The PVS powder acts as a monomer in the electrolyte. In the UV-visible spectrum of the graphite electrode, one absorption peak was observed at 222 nm that was also found for the PVS powder. This peak can be attributed to the PVS monomer molecules trapped in the SEI film polymer that formed on the surface of the graphite electrode [25]. In addition to the peak at 222 nm, a broad peak located at 255 nm can be seen in the spectrum of the graphite electrode that cycled in the PVS-containing electrolyte; this peak cannot be observed in the spectrum of the PVS powder. This peak can be attributed to the polymer film originating from the polymerization of the additive [44].

4. Conclusions

In this research, PVS was examined as a novel electrolyte additive for the improvement of the cycle stability of LIBs containing an EC-based electrolyte. The DFT calculations predicted that the PVS possesses higher RP and lower OP than EC, which findings were in agreement with the results obtained from the CV and LSV measurements. As evidenced by CV analysis, the SEI layer formed by the PVS can hamper the decomposition of the electrolyte. In addition, the cell with 1 wt % of the PVS demonstrated less interfacial and charge transfer resistance, which could result in a decrement in ohmic and also activation polarization in the intercalation/de-intercalation process of Li^+ ions into the electrode. As evidenced by Raman spectroscopy, the SEI formation process, occurring as the result of PVS reduction, led to less structural disorder in the graphite electrode, which could make it an appropriate additive for LIBs. According to the cycling performance analysis, a severe decline was observed in the capacity retention of the Li/graphite cell without PVS after 35 cycles. On the other hand, the cell with the PVS delivered superior cyclic stability with excellent capacity retention. Taking the abovementioned explanations into account, PVS may present a promising SEI additive for LIBs.

Supplementary Materials: The following supporting information can be downloaded at: https://www.mdpi.com/article/10.3390/en15176205/s1, Figure S1. Schematic representation of solid electrolyte interphase (SEI) formation in the potential range of 0.6–1.3 V vs. Li^+/Li and the role of SEI additives. Figure S2. Polymerization mechanism of SEI additives containing multiple bonds. Figure S3. The first charge/discharge cycle of Li/graphite half-cells with different contents of PVS in the voltage range of 0.001–3 V and the C-rate of 0.1 C.

Author Contributions: Conceptualization, B.M.; methodology, B.M.; software, B.M. and Z.S.; validation, B.M., M.J. and Z.S.; writing—original draft preparation, B.M.; writing—review and editing, B.M., M.J., Z.S. and M.A.; supervision, M.J. and Z.S.; project administration, M.J. and Z.S. All authors have read and agreed to the published version of the manuscript.

Funding: This research received no external funding.

Institutional Review Board Statement: Not applicable.

Informed Consent Statement: Not applicable.

Data Availability Statement: Not applicable.

Conflicts of Interest: The authors declare no conflict of interest.

References

1. Perveen, T.; Siddiq, M.; Shahzad, N.; Ihsan, R.; Ahmad, A.; Shahzad, M.I. Prospects in anode materials for sodium ion batteries-A review. *Renew. Sustain. Energy Rev.* **2020**, *119*, 109549. [CrossRef]
2. da Silva Lima, L.; Quartier, M.; Buchmayr, A.; Sanjuan-Delmás, D.; Laget, H.; Corbisier, D.; Mertens, J.; Dewulf, J. Life cycle assessment of lithium-ion batteries and vanadium redox flow batteries-based renewable energy storage systems. *Sustain. Energy Technol. Assess.* **2021**, *46*, 101286. [CrossRef]
3. Xiong, C.; Wang, T.; Zhang, Y.; Li, B.; Han, Q.; Li, D.; Ni, Y. Li–Na metal compounds inserted into porous natural wood as a bifunctional hybrid applied in supercapacitors and electrocatalysis. *Int. J. Hydrog. Energy* **2022**, *47*, 2389–2398. [CrossRef]

4. Xiong, C.; Li, M.; Han, Q.; Zhao, W.; Dai, L.; Ni, Y. Screen printing fabricating patterned and customized full paper-based energy storage devices with excellent photothermal, self-healing, high energy density and good electromagnetic shielding performances. *J. Mater. Sci. Technol.* **2022**, *97*, 190–200. [CrossRef]
5. Zhao, Y.; Fang, L.Z.; Kang, Y.Q.; Wang, L.; Zhou, Y.N.; Liu, X.Y.; Li, T.; Li, Y.X.; Liang, Z.; Zhang, Z.X.; et al. A novel three-step approach to separate cathode components for lithium-ion battery recycling. *Rare Met.* **2021**, *40*, 1431–1436. [CrossRef]
6. Moradi Bilondi, A.; Kermani, M.J.; Heidary, H.; Abdollahzadehsangroudi, M. Investigation of the Effect of Anode Fuel Contaminants on the Performance of Polymer Electrolyte Membrane Fuel Cell. *Amirkabir J. Mech. Eng.* **2020**, *52*, 381–398.
7. Chen, T.; Jin, Y.; Lv, H.; Yang, A.; Liu, M.; Chen, B.; Xie, Y.; Chen, Q. Applications of lithium-ion batteries in grid-scale energy storage systems. *Trans. Tianjin Univ.* **2020**, *26*, 208–217. [CrossRef]
8. Wang, S.; Ren, P.; Takyi-Aninakwa, P.; Jin, S.; Fernandez, C. A Critical Review of Improved Deep Convolutional Neural Network for Multi-Timescale State Prediction of Lithium-Ion Batteries. *Energies* **2022**, *15*, 5053. [CrossRef]
9. Urbańska, W.; Osial, M. Investigation of the Physico-Chemical Properties of the Products Obtained after Mixed Organic-Inorganic Leaching of Spent Li-Ion Batteries. *Energies* **2020**, *13*, 6732. [CrossRef]
10. Mosallanejad, B.; Malek, S.S.; Ershadi, M.; Daryakenari, A.A.; Cao, Q.; Ajdari, F.B.; Ramakrishna, S. Cycling degradation and safety issues in sodium-ion batteries: Promises of electrolyte additives. *J. Electroanal. Chem.* **2021**, *895*, 115505. [CrossRef]
11. Cheng, H.; Shapter, J.G.; Li, Y.; Gao, G. Recent progress of advanced anode materials of lithium-ion batteries. *J. Energy Chem.* **2021**, *57*, 451–468. [CrossRef]
12. Xia, S.; Wu, X.; Zhang, Z.; Cui, Y.; Liu, W. Practical challenges and future perspectives of all-solid-state lithium-metal batteries. *Chem* **2019**, *5*, 753–785. [CrossRef]
13. Liu, B.; Zhang, J.-G.; Xu, W. Advancing lithium metal batteries. *Joule* **2018**, *2*, 833–845. [CrossRef]
14. Cheng, X.-B.; Zhang, R.; Zhao, C.-Z.; Zhang, Q. Toward safe lithium metal anode in rechargeable batteries: A review. *Chem. Rev.* **2017**, *117*, 10403–10473. [CrossRef] [PubMed]
15. Zhang, H.; Yang, Y.; Ren, D.; Wang, L.; He, X. Graphite as anode materials: Fundamental mechanism, recent progress and advances. *Energy Storage Mater.* **2021**, *36*, 147–170. [CrossRef]
16. Beheshti, S.H.; Javanbakht, M.; Omidvar, H.; Hosen, M.S.; Hubin, A.; Van Mierlo, J.; Berecibar, M. Development, Retainment and Assessment of the Graphite-Electrolyte Interphase in Li-ion Batteries Regarding the Functionality of SEI-Forming Additives. *Iscience* **2022**, *25*, 103862. [CrossRef]
17. Song, H.-Y.; Jeong, S.-K. Investigating continuous co-intercalation of solvated lithium ions and graphite exfoliation in propylene carbonate-based electrolyte solutions. *J. Power Sources* **2018**, *373*, 110–118. [CrossRef]
18. Zhang, J.; Yang, J.; Yang, L.; Lu, H.; Liu, H.; Zheng, B. Exploring the redox decomposition of ethylene carbonate–propylene carbonate in Li-ion batteries. *Mater. Adv.* **2021**, *2*, 1747–1751. [CrossRef]
19. Haregewoin, A.M.; Wotango, A.S.; Hwang, B.-J. Electrolyte additives for lithium ion battery electrodes: Progress and per-spectives. *Energy Environ. Sci.* **2016**, *9*, 1955–1988. [CrossRef]
20. Zhang, S.S. A review on electrolyte additives for lithium-ion batteries. *J. Power Sources* **2006**, *162*, 1379–1394. [CrossRef]
21. Xu, K. Electrolytes and interphases in Li-ion batteries and beyond. *Chem. Rev.* **2014**, *114*, 11503–11618. [CrossRef] [PubMed]
22. Beheshti, S.H.; Javanbakht, M.; Omidvar, H.; Behi, H.; Zhu, X.; Mamme, M.H.; Hubin, A.; Van Mierlo, J.; Berecibar, M. Effects of structural substituents on the electrochemical decomposition of carbonyl derivatives and formation of the solid–electrolyte interphase in lithium-ion batteries. *Energies* **2021**, *14*, 7352. [CrossRef]
23. Lee, J.-T.; Lin, Y.-W.; Jan, Y.-S. Allyl ethyl carbonate as an additive for lithium-ion battery electrolytes. *J. Power Sources* **2004**, *132*, 244–248. [CrossRef]
24. Wagner, R.; Brox, S.; Kasnatscheew, J.; Gallus, D.R.; Amereller, M.; Cekic-Laskovic, I.; Winter, M. Vinyl sulfones as SEI-forming additives in propylene carbonate based electrolytes for lithium-ion batteries. *Electrochem. Commun.* **2014**, *40*, 80–83. [CrossRef]
25. Komaba, S.; Itabashi, T.; Tatsuya Ohtsuka, H.; Groult, N.; Kumagai, N.; Kaplan, B.; Yashiro, H. Impact of 2-vinylpyridine as electrolyte additive on surface and electrochemistry of graphite for C/$LiMn_2O_4$ Li-ion Cells. *J. Electrochem. Soc.* **2005**, *152*, A937. [CrossRef]
26. Frisch, M.J.; Trucks, G.W.; Schlegel, H.B.; Scuseria, G.E.; Robb, M.A.; Cheeseman, J.R.; Scalmani, G.; Barone, V.; Petersson, G.A.; Nakatsuji, H.; et al. *Gaussian 09, Revision A.02*; Gaussian, Inc.: Wallingford, CT, USA, 2009.
27. Mosallanejad, B. Phthalimide Derivatives: New Promising Additives for Functional Electrolyte in Lithium-ion Batteries. *Chem. Methodol.* **2019**, *3*, 261–275.
28. Li, X.; Yin, Z.; Li, X.; Wang, C. Ethylene sulfate as film formation additive to improve the compatibility of graphite electrode for lithium-ion battery. *Ionics* **2014**, *20*, 795–801. [CrossRef]
29. Li, B.; Xu, M.; Li, B.; Liu, Y.; Yang, L.; Li, W.; Hu, S. Properties of solid electrolyte interphase formed by prop-1-ene-1,3-sultone on graphite anode of Li-ion batteries. *Electrochim. Acta* **2013**, *105*, 1–6. [CrossRef]
30. Fu, Y.; Chen, C.; Qiu, C.; Ma, X. Vinyl ethylene carbonate as an additive to ionic liquid electrolyte for lithium ion batteries. *J. Appl. Electrochem.* **2009**, *39*, 2597–2603. [CrossRef]
31. Wang, R.; Li, X.; Wang, Z.; Zhang, H. Electrochemical analysis graphite/electrolyte interface in lithium-ion batteries: P-Toluenesulfonyl isocyanate as electrolyte additive. *Nano Energy* **2017**, *34*, 131–140. [CrossRef]
32. Li, Y.; Chen, X.; Dolocan, A.; Cui, Z.; Xin, S.; Xue, L.; Xu, H.; Park, K.; Goodenough, J.B. Garnet electrolyte with an ultralow interfacial resistance for Li-metal batteries. *J. Am. Chem. Soc.* **2018**, *140*, 6448–6455. [CrossRef] [PubMed]

33. Yan, G.; Li, X.; Wang, Z.; Guo, H.; Wang, J. Compatibility of graphite with 1,3-(1,1,2,2-Tetrafluoroethoxy) propane and fluoroethylene carbonate as cosolvents for nonaqueous electrolyte in lithium-ion batteries. *J. Phys. Chem. C* **2014**, *118*, 6586–6593. [CrossRef]
34. Xu, M.Q.; Li, W.S.; Zuo, X.X.; Liu, J.S.; Xu, X. Performance improvement of lithium ion battery using PC as a solvent component and BS as an SEI forming additive. *J. Power Sources* **2007**, *174*, 705–710. [CrossRef]
35. Hu, Y.; Kong, W.; Li, H.; Huang, X.; Chen, L. Experimental and theoretical studies on reduction mechanism of vinyl ethylene carbonate on graphite anode for lithium ion batteries. *Electrochem. Commun.* **2004**, *6*, 126–131. [CrossRef]
36. Ota, H.; Kominato, A.; Chun, W.-J.; Yasukawa, E.; Kasuya, S. Effect of cyclic phosphate additive in non-flammable electrolyte. *J. Power Sources* **2003**, *119*, 393–398. [CrossRef]
37. Choi, N.-S.; Profatilova, I.A.; Kim, S.-S.; Song, E.-H. Thermal reactions of lithiated graphite anode in LiPF6-based electrolyte. *Thermochim. Acta* **2008**, *480*, 10–14. [CrossRef]
38. Wang, L.; Menakath, A.; Han, F.; Wang, Y.; Zavalij, P.Y.; Gaskell, K.J.; Borodin, O.; Iuga, D.; Brown, S.P.; Wang, C.; et al. Identifying the components of the solid–electrolyte interphase in Li-ion batteries. *Nat. Chem.* **2019**, *11*, 789–796. [CrossRef]
39. Xing, M.L.; Li, W. Interphases between electrolytes and anodes in Li-ion battery. In *Electrolytes for Lithium and Lithium-Ion Batteries*; Jow, T.R., Xu, K., Borodin, O., Ue, M., Eds.; Springer: New York, NY, USA, 2014; pp. 227–277.
40. Wadher, S.J.; Puranik, M.P.; Karande, N.A.; Yeole, P.G. Synthesis and biological evaluation of Schiff base of dapsone and their derivative as antimicrobial agents. *Int. J. PharmTech Res.* **2009**, *1*, 22–33.
41. Puro, L.; Mänttäri, M.; Pihlajamäki, A.; Nyström, M. Characterization of modified nanofiltration membranes by octanoic acid permeation and FTIR analysis. *Chem. Eng. Res. Des.* **2006**, *84*, 87–96. [CrossRef]
42. Markervich, E.; Salitra, G.; Levi, M.D.; Aurbach, D. Capacity fading of lithiated graphite electrodes studied by a combination of electroanalytical methods, Raman spectroscopy and SEM. *J. Power Sources* **2005**, *146*, 146–150. [CrossRef]
43. Sethuraman, V.A.; Hardwick, L.J.; Srinivasan, V.; Kostecki, R. Surface structural disordering in graphite upon lithium intercalation/deintercalation. *J. Power Sources* **2010**, *195*, 3655–3660. [CrossRef]
44. Li, B.; Wang, Y.; Lin, H.; Wang, X.; Xu, M.; Wang, Y.; Xing, L.; Li, W. Performance improvement of phenyl acetate as propylene carbonate-based electrolyte additive for lithium ion battery by fluorine-substituting. *J. Power Sources* **2014**, *267*, 182–187. [CrossRef]